How Momentum Coupling Affects SST Variance and Large-Scale Pacific Climate Variability in CESM

SARAH M. LARSON AND DANIEL J. VIMONT

Atmospheric and Oceanic Sciences Department, and Nelson Institute Center for Climatic Research, University of Wisconsin–Madison, Madison, Wisconsin

AMY C. CLEMENT AND BEN P. KIRTMAN

Rosenstiel School of Marine and Atmospheric Science, University of Miami, Miami, Florida

(Manuscript received 26 September 2017, in final form 7 January 2018)

ABSTRACT

The contribution of buoyancy (thermal + freshwater fluxes) versus momentum (wind driven) coupling to SST variance in climate models is a longstanding question. Addressing this question has proven difficult because a gap in the model hierarchy exists between the fully coupled (momentum + buoyancy + ocean dynamics) and slab–mixed layer ocean coupled (thermal with no ocean dynamics) versions. The missing piece is a thermally coupled configuration that permits anomalous ocean heat transport convergence decoupled from the anomalous wind stress. A mechanically decoupled model configuration is provided to fill this gap and diagnose the impact of momentum coupling on SST variance in NCAR CESM. A major finding is that subtropical SST variance increases when momentum coupling is disengaged. An ''opposing flux hypothesis'' may explain why the subtropics (midlatitudes) experience increased (reduced) variance without momentum coupling. In a subtropical easterly wind regime, Ekman fluxes (Q'_{ek}) oppose thermal fluxes (Q'_{th}), such that when the air and sea are mechanically decoupled ($Q'_{ek} = 0$), $Q'_{ek} + Q'_{th}$ variance increases. As a result, SST variance increases. In a midlatitude westerly regime where Q'_{ek} and Q'_{th} typically reinforce each other, SST variance is reduced. Changes in mean surface winds with climate change could impact the Q'_{ek} and Q'_{th} covariance relationships. A by-product of mechanically decoupling the model is the absence of ENSO variability. The Pacific decadal oscillation operates without momentum coupling or tropical forcing, although the pattern is modified with enhanced (reduced) variability in the subtropics (midlatitudes). Results show that Ekman fluxes are an important component to tropical, subtropical, and midlatitude SST variance.

1. Introduction

Atmosphere–ocean coupling is no doubt an important component of the climate system. How models simulate SST variability, for example, depends on what coupled processes are considered in the model (e.g., Lau and Nath 1996; Manabe and Stouffer 1996; Barsugli and Battisti 1998; Bladé 1999; Alexander and Scott 2008). Of particular interest is the impact of atmosphere–ocean coupling on SST variance, as variability in surface temperature imparts both local and remote impacts on the atmospheric circulation (Lau and Nath 2003; Wu and Kirtman 2005).

In the midlatitudes, air–sea heat fluxes are the primary driver of SST variability [see reviews by Frankignoul (1985) and Neelin et al. (1994)] and the rich body of literature supplies a variety of approaches to support this notion using both simplified (Barsugli and Battisti 1998) and coupled models (Manabe and Stouffer 1996; Bladé 1999; Fan and Schneider 2012). For instance, Manabe and Stouffer (1996) find similar midlatitude surface air temperature variance at low frequencies in two atmosphere general circulation model (GCM) configurations, one coupled to an ocean GCM and one coupled to a slab–mixed layer ocean model (SOM). Similar results in these two versions suggest that thermal coupling is more important than momentum coupling in the midlatitudes, as the SOM does not include wind-driven ocean dynamics. In the tropics, however, the primary driver of SST variability is surface wind stress (i.e., momentum coupling), with thermal fluxes playing a secondary damping role (Neelin et al. 1994). When

Corresponding author: Sarah M. Larson, slarson28@wisc.edu

DOI: 10.1175/JCLI-D-17-0645.1

developed theory and computational capabilities first facilitated in-depth coupling studies, most model experiments were performed with AGCMs coupled to SOMs, leaving little opportunity to diagnose the contribution of wind-driven effects on SST variance.

Similar methodological approaches to study the effects of coupling on SST variability in the subtropics are less common. Instead, studies focus on phenomenological features generating SST variability, including meridional modes (Chiang and Vimont 2004; Zhang et al. 2014) and interactions between the tropics and extratropics (Alexander 1992; Lau and Nath 1994, 1996, 2001; Gu and Philander 1997; Zhang et al. 1998; Kleeman et al. 1999; Klein et al. 1999; Vimont et al. 2001, 2003; Alexander et al. 2002; Solomon et al. 2003; Alexander et al. 2010). Although several of such studies argue that the wind–evaporation–SST feedback (Xie and Philander 1994) is an important thermodynamic driver of subtropical SST variability, the broad effect of momentum coupling is not known. The goal of this study is to provide a global perspective on the effects of momentum coupling on SST variance.

Current-day climate models include fully dynamical atmosphere and ocean models and both buoyancy and momentum coupling to represent communication between the two components. Buoyancy coupling includes sensible and latent fluxes to represent heat exchange between the atmosphere and ocean, as well as freshwater fluxes. Momentum coupling allows for momentum fluxes from the atmosphere to force the ocean surface, driving Ekman advection, entrainment, and other wind-driven processes that influence SST. All the while, the atmosphere responds to the ocean SST with either a reinforcing or damping effect.

As models become increasingly complex, it is important to take a step back and refocus on individual processes contributing to the overall variability, including atmosphere–ocean coupling. Understanding how coupling contributes to SST variability can be pursued through model experiments that ''switch off'' components of the air–sea coupling. For example, the ''interactive ensemble'' approach decouples weather noise by forcing one ocean model with the ensemble mean of multiple AGCM realizations, whereas each AGCM realization is forced by the same ocean (Kirtman and Shukla 2002). Another approach is integrating complementary fully coupled and SOM versions and then comparing the SST anomaly statistics (e.g., Manabe and Stouffer 1996; Bladé 1999). Persistent SST variability in the SOM is considered to be a response to thermal coupling whereas the fully coupled version includes wind-driven effects. One of the main hesitations in comparing the SOM with the fully coupled version is in the role of ocean dynamics. For example, there is debate about whether the role of ocean dynamics is important for Atlantic multidecadal variability that stems from similarities in the SOM and fully coupled versions (Clement et al. 2015; Zhang et al. 2016). An important open question is whether the ocean dynamics dampen or enhance the thermally driven SST response. Whether extratropical surface climate is mechanically, thermally, or tropically driven remains a longstanding question because the effects of wind-driven ocean dynamics are not easily separable from the thermally coupled component in current-day models.

To our knowledge, there is little information in the literature quantifying the extent to which SST variance is driven by thermal fluxes in the present of anomalous ocean heat transport convergence decoupled from the anomalous wind stress (hereafter τ). In other words, the exact role momentum coupling plays in the simulated SST variability in climate models is not obvious. In this study, we attempt to reconcile this gap in knowledge by utilizing a mechanically decoupled version of a climate model (Larson and Kirtman 2015b), a configuration that sits in the middle of the model hierarchy between the fully coupled and SOM approaches. Using this approach, we switch off the momentum coupling and diagnose the climate response by focusing on the changes in SST variance and large-scale Pacific SST anomaly (SSTA) variability. More simply, we show what happens to the SST variance when anomalous τ cannot mechanically drive changes in the ocean circulation, leaving thermal fluxes and anomalous ocean heat transport convergence decoupled from the anomalous τ as the primary drivers of SST variability. This paper is organized as follows. Section 2 introduces the model simulations. Section 3 highlights regions where SST variance is reduced in the mechanically decoupled model. Section 4 highlights regions of enhanced variance and introduces two hypotheses as explanation. How momentum coupling influences the Pacific decadal oscillation is discussed in section 5. Section 6 summarizes results, discusses implications for SOM models, and suggests potential ideas for climate change scenario studies using the mechanically decoupled model configuration.

2. Climate models and methodology

a. CESM fully coupled control

The control model is the National Center for Atmospheric Research (NCAR) Community Earth System Model version 1.2.0 (CESM; Hurrell et al. 2013). CESM consists of land, cryosphere, atmosphere, and ocean models, each communicating through a flux coupler. In

this configuration, the Parallel Ocean Program version 2 (POP2) is coupled to the Community Atmosphere Model version 4 through the CESM flux coupler version 7. CESM is integrated with preindustrial forcing at a nominal 1° horizontal resolution. POP2 consists of 60 vertical levels, with higher-resolution 10-m increments in the upper 160 m of the ocean (Danabasoglu et al. 2012). CESM control is integrated for 680 years and the last 300 years are utilized for analyses. Hereafter, any reference to the ''control'' refers to the fully coupled CESM.

Much of the present study will focus on Pacific SST. Relevant details in Deser et al. (2012) for the predecessor of CESM, the Community Climate System Model version 4 (CCSM4; Gent et al. 2011; Bates et al. 2012) are mentioned to describe the fidelity of the model. Since the analyses focus on ocean and atmosphere variables, CCSM4 is an appropriate analog as it is configured with similar components as the CESM version used here. CCSM4 simulates a realistic Pacific decadal oscillation (PDO; Zhang et al. 1997) yet with weaker-than-observed projection onto the tropical Pacific. Similar to observations, CCSM4 simulates a PDO with a red spectrum. ENSO spatial structure and variability are realistic, although the standard deviation is ~30% too large. In the Southern Ocean, CCSM4 simulates a realistic southern annual mode spatial pattern but is too zonally symmetric compared to reanalysis products (Weijer et al. 2012). Pacific SST variability studies on a variety of topics including ENSO (Deser et al. 2012; Capotondi 2013; DiNezio and Deser 2014), meridional modes (Zhang et al. 2014; Thomas and Vimont 2016), decadal and longer time scale variability (Karnauskas et al. 2012; Meehl et al. 2013; Okumura 2013), climate prediction and predictability (Larson and Kirtman 2014, 2015b, Kirtman et al. 2014), and climate change (Stevenson et al. 2012) have utilized CCSM4/CESM either fully coupled or the SOM version (Bitz et al. 2012); therefore, CESM is deemed an appropriate tool for this SST variance study. The reader is referred to the CCSM4 Special Collections edition available at http://journals.ametsoc.org/topic/ccsm4-cesm1.

b. A mechanically decoupled CESM

CESM1.2.0 is also integrated in a mechanically decoupled (MD) configuration. The MD configuration was designed in Larson and Kirtman (2015b) for CCSM4 and the code was updated for CESM in an annual cycle model bias study (Larson et al. 2017). The goal of the MD is to disable the mechanical effects of anomalous τ forcing on the ocean while retaining other advantages of a fully coupled model, including unconstrained buoyancy (thermal + freshwater) fluxes, atmosphere dynamics, ocean dynamics (except for the component driven by anomalous τ), mean ocean circulation, and a freely evolving mixed-layer depth. This is achieved by allowing the ocean model to experience only climatological τ,as a result, only the annual cycle of momentum fluxes forces the ocean component. Therefore, the ocean feels no anomalous momentum fluxes, which means that anomalous τ cannot mechanically drive changes in ocean circulation. As such, anomalous τ cannot drive a slew of processes including anomalous Ekman advection, ocean mixing, coupled atmosphere–ocean dynamical feedbacks (e.g., Bjerknes feedback), subtropical cells (McCreary and Lu 1994), trade wind charging of the equatorial Pacific (Anderson 2007), variability in western boundary currents (e.g., DiNezio et al 2009), and ENSO, among others. The reader is referred to Larson and Kirtman (2015b) for ENSO diagnostics of the MD CCSM4.

Within the model infrastructure, the flux coupler passes atmosphere model-derived τ to the ocean model once per model day. At this time, the code overwrites the model-derived τ with control CESM monthly mean climatology. Larson et al. (2017) show that using daily climatological τ versus allowing every day of the respective month to experience the same monthly mean climatology has minimal effect on the monthly mean SST seasonal cycle in the eastern Pacific. Therefore, we choose the more computationally efficient monthly mean version. To be clear, the atmosphere model freely evolves and produces τ that is used in the thermal flux calculations. The ocean does not experience this version of the τ but does feel the associated thermal fluxes. The MD is branched from year 680 of the control simulation and integrated for 300 years to compare with the control. The MD has since been extended for an additional 200 years and results remain unchanged (not shown).

The MD sits between the fully coupled and SOM versions in the model hierarchy. The SOM includes a fixed mixed layer depth (MLD) that is thermodynamically coupled to the atmosphere model. The MD MLD, however, freely responds to changes in buoyancy fluxes, the annual cycle of τ, and anomalous ocean mass transport decoupled from the anomalous τ. The MLD in the fully coupled version also responds to anomalous τ forcing. The MD differs from the fully coupled version in that the ocean does not feel anomalous τ but does feel the associated heat fluxes.

The MD, by design, includes the annual cycle of momentum fluxes forcing the ocean, and thus the climatological mean ocean circulation is represented. Moreover, the full equations of motion for the ocean remain intact, although contributions to the variability cannot arise from anomalous τ-driven momentum fluxes. More simply,

ocean variability apart from the annual cycle in the MD can arise from two sources, buoyancy fluxes and anomalous ocean mass transport decoupled from the anomalous τ. As the present study focuses on SSTA, mechanisms that contribute to SST variability are of particular interest. Results from the MD represent what happens to the SST variance when anomalous τ cannot mechanically drive changes in the ocean circulation, leaving thermal fluxes and anomalous ocean heat transport convergence decoupled from the anomalous τ as the primary drivers of SST variability. Sources of the latter include mean advection of anomalous ocean temperature, buoyancy-driven circulation, mixing, and shear instabilities (e.g., tropical instability waves driven by the mean current shear), among others. Comparing the MD with the control allows us to decipher what role momentum coupling plays in the simulated SST variability in the fully coupled model.

An advantage of the MD is to model climate variability in the absence of ENSO, a challenge that has been attempted with mathematical extraction techniques and modeling efforts in the past. Typical analysis methods to isolate or remove ENSO include composite averaging neutral ENSO years (Goodrich 2007), linear regression (Blanke et al. 1997; Chiang and Vimont 2004; Larson and Kirtman 2013), and various filtering techniques (Kug et al. 2008; Jin and Kirtman 2009; Compo and Sardeshmukh 2010), but these are not without caveats. Delayed responses to ENSO can contaminate composite and regression results. The nonlinear tails of ENSO may remain as statistical artifacts when using regression methods. Bandpass filtering may remove important non-ENSO interannual variability. Several modeling studies prescribe tropical Pacific climatological SST to manually remove ENSO (Lau and Nath 1994, 1996; Bladé 1999). These experiments lack a dynamical ocean and, by design, lack thermodynamic coupling where SST is prescribed. Others use a slab model to exclude ENSO dynamics (Clement et al. 2011; Thomas and Vimont 2016), although this removes the effects of ocean dynamics. One SOM has been shown to simulate ENSO variability (Dommenget 2010), although this a unique response resulting from the model's equatorial Pacific mean state facilitating unstable atmospheric feedbacks. By design, the MD eliminates tropically driven (i.e., ENSO) effects on global variability. Although removing ENSO was the goal in Larson and Kirtman (2015b), in the context of the present study one should think of the elimination of ENSO as a by-product of mechanically decoupling the model.

It is worthwhile to briefly mention how the MD can be used to address a variety of science questions. In a series of ENSO predictability papers, Larson and Kirtman (2015a,b, 2017a,b) use the MD as a means to produce initial conditions that are forced with identical τ but vary slightly due to atmospheric and oceanic "noise." For example, the MD as described herein is perpetually ENSO-neutral. To quantify coupled instability-induced perturbation growth important for ENSO predictions, Larson and Kirtman (2015b) branch simulations from every first of January, March, May, July, and September of the MD for 30 years and turn the coupling back on (i.e., run fully coupled), creating ensembles representing noise-driven perturbation growth. Larson and Kirtman (2017b) then quantify how the perturbation growth statistics and ENSO predictability change when the initial condition includes a subsurface recharge/discharge (Jin 1997). In an annual cycle study, Larson et al. (2017) use the MD version herein and several other variations including a simulation in which the ocean only experiences annual mean climatological τ to decompose the wind-driven SST and precipitation errors in the eastern equatorial Pacific annual cycle in CCSM/CESM.

c. SST variance

The MD SST climatology is only modestly different from the control. The control seasonal SST climatology is shown in Fig. 1. In the annual mean SST, the MD is slightly warmer than the fully coupled in the midlatitudes and cooler in the eastern equatorial Pacific (also see Larson et al. 2017). The warming in the Northern Hemisphere (NH) midlatitudes occurs primarily during boreal summer, whereas the warming in the Southern Hemisphere (SH) occurs in boreal winter.

To summarize the differences in the MD SST variability compared to the control, Fig. 2a shows the variance ratio calculated at each grid point:

$$\mathrm{VR}_{\mathrm{SST}} = \frac{\sigma^2_{\mathrm{MD}}}{\sigma^2_{\mathrm{control}}}, \tag{1}$$

where σ^2_α is the SSTA variance of simulation α. A value of $\mathrm{VR}_{\mathrm{SST}} < 1$ indicates regions where the MD variance is reduced compared to the control, $\mathrm{VR}_{\mathrm{SST}} \approx 1$ indicates little to no change, and $\mathrm{VR}_{\mathrm{SST}} > 1$ indicates increased variance in the MD. Areas of robust reduced and enhanced variance are highlighted in subsequent sections. SST variance is reduced nearly everywhere in the global ocean, except for the Pacific subtropics and, to a lesser extent, the Atlantic subtropics (we do not focus herein on large changes in $\mathrm{VR}_{\mathrm{SST}}$ near ice margins). Figures 2b and 2c show the zonally averaged $\mathrm{VR}_{\mathrm{SST}}$ encompassing the increased variance regions in the Pacific, stratified by calendar month. In Fig. 2b, $\mathrm{VR}_{\mathrm{SST}}$ is averaged over 140°E–120°W to capture the NH subtropical Pacific and in Fig. 2c, over 120°–80°W to capture the SH subtropical

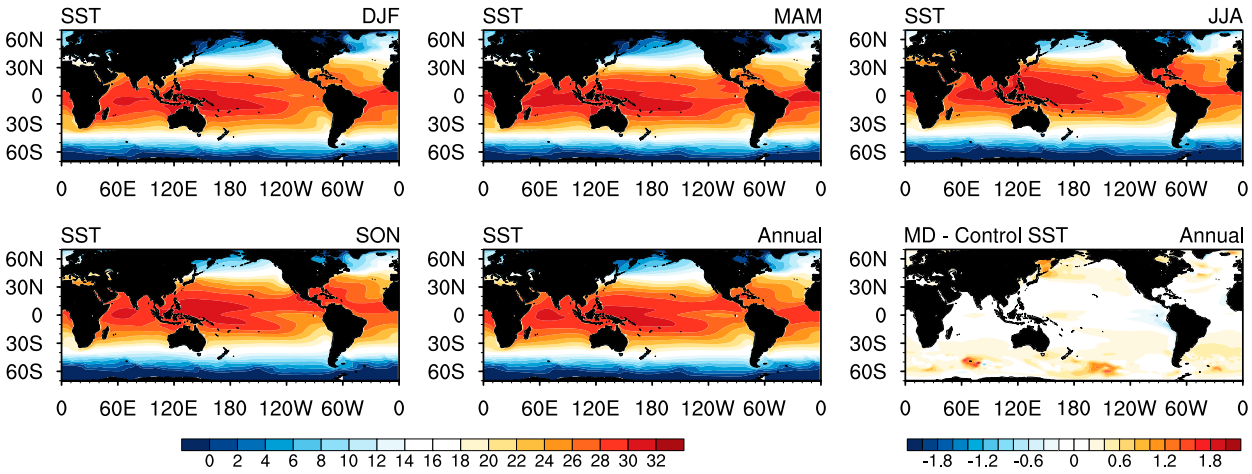

FIG. 1. CESM fully coupled control SST climatology for December–February (DJF), March–May (MAM), June–August (JJA), September–November (SON), and the annual mean in °C. Bottom right shows the annual mean CESM MD SST minus the annual mean control SST.

Pacific. The value of VR_{SST} varies with the seasonal cycle, with the NH maximizing in boreal spring–summer and the SH in boreal summer–fall, consistent with when the climatological meridional SST gradient is largest in these regions as in Figs. 2d–f (see also Fig. 1). As will be demonstrated in section 4b, the climatological meridional SST gradient is a key term in the anomalous wind-driven Ekman flux equation, which is an important contributor to SST variance (e.g., Alexander 1992).

3. Reduced SST variance

The majority of the World Ocean experiences a reduction in SST variance when momentum coupling is disengaged. A reduction in SST variance means that mechanical coupling (i.e., τ variability forcing the ocean) is necessary to simulate the full control variability and that buoyancy fluxes and anomalous ocean heat transport convergence decoupled from anomalous τ together cannot explain the fully coupled control variability. To explain the reduced SST variance in certain regions, this section focuses on region-specific processes eliminated when the model is mechanically decoupled.

a. Equatorial eastern Pacific

The equatorial Pacific SST variance is reduced for obvious reasons related to the suppression of ENSO variability. Similar to the CCSM4 MD (Larson and Kirtman 2015b), the CESM MD also exhibits no canonical ENSO variability. Figure 3 displays the Niño-3 (averaged over 5°S–5°N, 150°–90°W) SSTA time series and the respective Pacific SSTA spatial regression patterns. The control time series shows large interannual variability. The spatial structure is a canonical ENSO pattern. The MD time series and spatial pattern show no evidence of canonical ENSO variability but instead show a weak amplitude SST pattern in the southeast Pacific with a predominantly red spectrum (not shown). The standard deviation of the MD Niño-3 time series is 0.1°C compared to roughly 1.0°C for the fully coupled model.

The MD SST pattern is reminiscent of that associated with decadal SST variability in the equatorial Pacific (Trenberth and Hurrell 1994; Zhang et al. 1997; Yeh and Kirtman 2004; Vimont 2005; Clement et al. 2011; Chen and Wallace 2015; Di Lorenzo et al. 2015) as well as the South Pacific meridional mode (Zhang et al. 2014). While the origin of equatorial Pacific decadal variability is debated, resulting from either random variations in interannual ENSO variability (Newman et al. 2003; Vimont 2005), ocean processes (Knutson and Manabe 1998; Kirtman 1997), stochastic forcing (Yeh and Kirtman 2004), or thermal coupling (Clement et al. 2011; Zhang et al. 2014), here we focus on insight that can be inferred from the MD. Describing the MD variability as "ENSO-like" (Chen and Wallace 2015) is inappropriate considering that the pattern cannot arise via the traditional coupled dynamics of ENSO theory (Zebiak and Cane 1987; Jin 1997). The MD pattern also differs from so-called ENSO-like variability in previous studies, as no robust North Pacific signals accompany the tropical SSTA pattern. Previously, Larson and Kirtman (2015b) reported that no such variability occurs in the MD CCSM4. This is unsurprising considering that the amplitude is roughly half that found in CCSM4-SOM (L. Murphy 2016, personal communication). Nevertheless, a weak Niño-3 pattern is seen in the MD and is definitively independent of ENSO. This does not refute

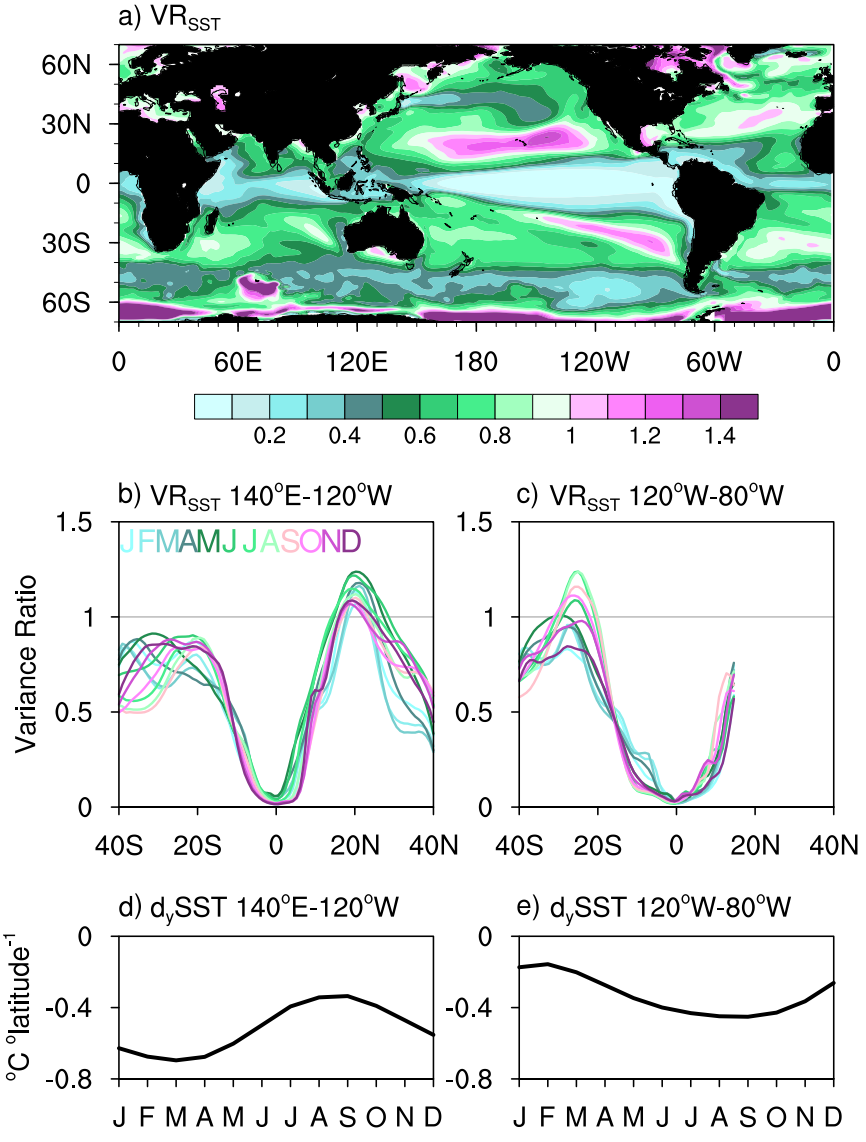

FIG. 2. (a) Unfiltered SSTA variance ratio VR_{SST} calculated as the variance of SSTA in the mechanically decoupled (MD) CESM divided by that of the CESM fully coupled control. Variance is computed over time at each grid point. Values > 1 (purples) indicate increased variance in the MD. (b),(c) VR_{SST} zonally averaged over 140°E–120°W and 120°–80°W, respectively, colored by calendar month. (d) Control meridional SST gradient climatology computed by subtracting the climatological SST at 20°N from 35°N and averaged over the longitudes in (b). (e) Control meridional SST gradient climatology computed by subtracting the climatological SST at 20°S from 35°S and averaged over the longitudes in (c).

previous studies arguing that equatorial Pacific decadal variability is largely due to variations in interannual ENSO variability (Newman et al. 2003; Vimont 2005), but it does suggest there exists a low-amplitude eastern Pacific pattern driven by either internal ocean processes (Yeh and Kirtman 2006) or thermal fluxes in CESM. Since anomalous winds cannot generate Ekman advection, upwelling, or equatorial waves, thermal flux forcing is likely driving the Niño-3 pattern, consistent with that seen in SOMs (Dommenget 2010; Clement et al. 2011; Zhang et al. 2014), although teasing out the exact mechanism is left for future study. The 0.1°C Niño-3 standard deviation is also seen in the CCSM4 MD. This suggests that CCSM4-SOM may be overestimating the thermally driven component of the Niño-3 pattern and that the combination of a seasonally varying MLD and anomalous ocean heat transport convergence decoupled from anomalous τ like that in the MD may be important

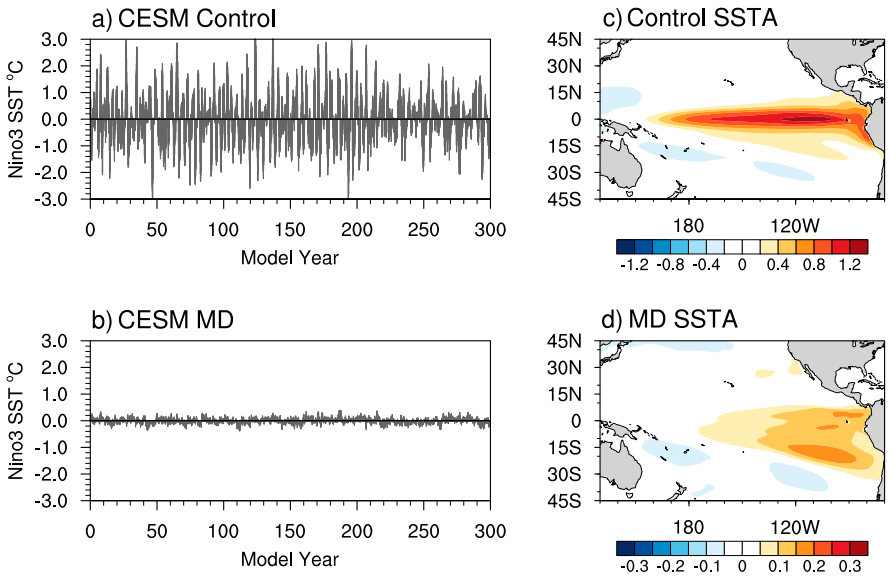

FIG. 3. Niño-3 SSTA index for the (a) CESM fully coupled control and (b) CESM MD, and regression of unfiltered SST anomalies onto the Niño-3 SST anomaly index for (c) control and (d) MD. Note different min/max on the color bars.

to properly quantify the amplitude of the thermally driven component of this pattern. The higher-amplitude decadal variability seen in observations must be a combination of momentum coupling in addition to the thermally driven component.

b. *Global tropics*

Along the equatorial band where anomalous τ is the primary driver of SST variability (Bjerknes 1969), SST variance is reduced by 50%–90% in all basins in the MD (Fig. 2a). One can assume that the reduced variance is, in part, due to the lack of ENSO and ENSO teleconnections (Trenberth et al. 1998; Alexander et al. 2002). Variations in the Walker circulation strength and associated changes in Ekman transport as well as weather noise τ also do not contribute to SST variance in the MD. Figure 4 shows the zonally averaged zonal τ anomaly variance ratio ($\sigma^2_{\mathrm{MD,taux}}/\sigma^2_{\mathrm{control,taux}}$) computed over the date line, the Pacific basin, and globally using only ocean grid points. For the MD, the τ considered originates from the atmosphere model-derived output, not the prescribed climatology forcing the ocean. Zonal τ variance over the equatorial date line is reduced by nearly 80%, as this region is strongly linked to ENSO variability. The full Pacific basin shows over a 60% reduction in zonal τ variance over the equator and a nearly 40% reduction occurs over the equatorial global ocean. Note that the variance ratio poleward of 20°–30° in both hemispheres converges toward 1.0, meaning that most zonal τ variance is maintained away from the tropics. Results indicate that the majority of zonal τ variance in the extratropics in CESM originates from mechanically decoupled atmospheric variability, which includes the atmospheric response to SST variability and the stochastic component. Variability in the upper and lower branches of both the Walker and Hadley circulations in the Pacific is reduced by 70%–90% (not shown), presumably due to the lack of ENSO variability.

c. *Southern Ocean*

Reduced SST variance also occurs between 40° and 60°S in the Southern Ocean. One possibility is that the

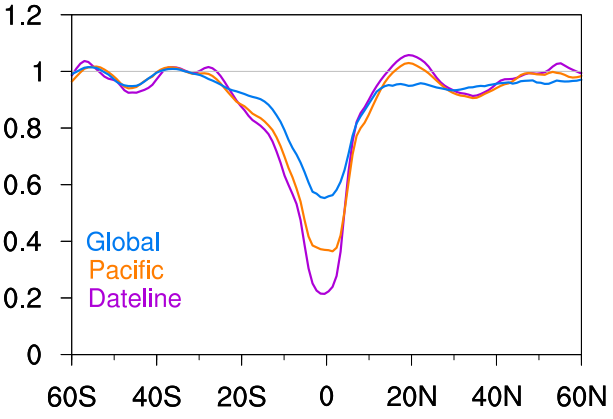

FIG. 4. Latitudinal profile of the zonal τ anomaly variance ratio (MD/control) zonally averaged over all global ocean data points, the Pacific basin only, and over the date line. The τ is the atmosphere model-derived zonal τ.

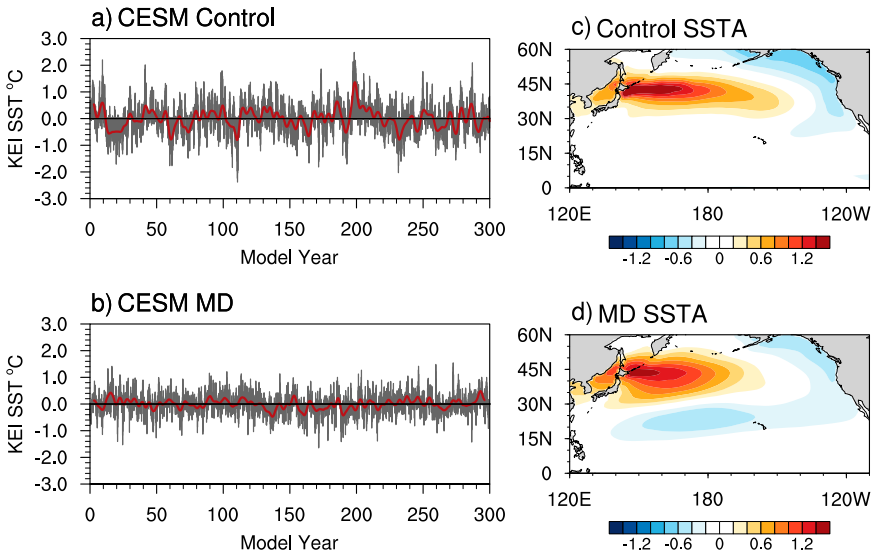

FIG. 5. The Kuroshio–Oyashio Extension Index (KEI) defined in Kwon and Deser (2007) as the area-averaged SSTA over 35°–45°N, 140°–180°E for (a) the fully coupled control and (b) the MD (in gray). The low-pass filtered (Lanczos filter with 13-yr cutoff) KEI is shown in red. Also shown is the regression of unfiltered SST anomalies onto the KEI for (c) the control and (d) MD.

atmospheric variability associated with the southern annual mode (SAM; Rogers and van Loon 1982; Hartmann and Lo 1998; Limpasuvan and Hartmann 1999; Thompson and Wallace 2000) cannot drive anomalous Ekman transport and eddies that influence the SST through the redistribution of heat (Meredith and Hogg 2006; Hogg et al. 2008; Screen et al. 2009). Another possibility is the lack of weather τ associated with storm tracks and the variability in the position of the ice edge. Diagnosing the impact of momentum coupling on ocean circulation and sea ice is a worthy topic but left for a future study.

d. North Pacific

The North Pacific is another region of robust reduction in SST variance. The reduced variance stemming from the northwest Pacific is indicative of reduced SST variability associated with the Kuroshio–Oyashio Extension (KE). Yeh et al. (2007) demonstrate through "interactive ensemble" model experiments that atmospheric variability significantly contributes to SSTA variance in the KE region. Furthermore, Kwon and Deser (2007) argue that basin-scale anomalous τ curl in the presence of atmosphere–ocean coupling is the primary mechanism forcing decadal KE variability in CCSM2, a predecessor of CCSM4. This idea is also expressed in earlier studies with reanalysis products (Deser et al. 1999) and simpler models (Schneider et al. 2002). Anomalous Ekman pumping is important for setting the decadal time scale (Ferreira et al. 2001) by exciting westward propagating Rossby waves (Deser et al. 1999; Schneider et al. 2002) and can shift the meridional location of the gyre boundary (Schneider et al. 2002). The common forcing mechanism described in this body of literature is alterations in τ (Miller et al. 1998; Seager et al. 2001; Schneider et al. 2002; Wu et al. 2003; Yeh et al. 2007; Liu 2012).

Following Kwon and Deser (2007), we compute a KE index (KEI) defined as the area-averaged SSTA over 35°–45°N, 140°E–180° to generate an SSTA time series (Fig. 5). The control shows low-frequency variability on decadal time scales, whereas the decadal variability in the MD appears damped. The standard deviation of the control time series is 0.6°C compared to the MD at 0.4°C. The power spectrum (not shown) reveals that the reduced variability in this region is almost exclusively in frequencies longer than one cycle per 8 years, confirming that anomalous τ is the vital forcing mechanism for decadal KE variability (Miller et al. 1998; Deser et al. 1999; Seager et al. 2001; Schneider et al. 2002; Qiu 2003).

For completeness, other plausible reasons for reduced North Pacific SST variance in the MD include 1) the lack of ENSO teleconnections (Weare et al. 1976; Pierce et al. 2001; Newman et al. 2003; Rodgers et al. 2004; Vimont 2005; Schopf and Burgman 2006), 2) the lack of Aleutian low variability or synoptic weather winds driving anomalous ocean advection and mixing, or 3) mixed-layer processes such as the "reemergence" mechanism (Alexander and Deser 1995) having less influence on SST without an ENSO-driven component

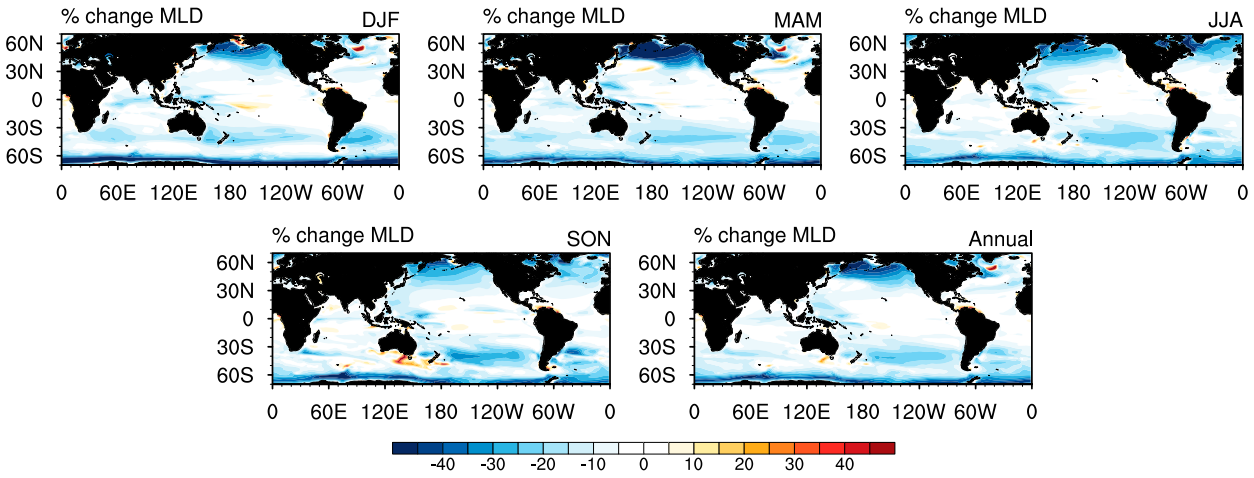

FIG. 6. Annual mean mixed layer (MXL) depth difference between the fully coupled control and the MD. Negative (positive) MXL anomalies indicate a shallower (deeper) MXL in the MD.

in the North Pacific. For reasons 2 and 3, associated thermal fluxes and the annual cycle of τ can force the SST and contribute to these mechanisms, although no thermal fluxes associated with ENSO occur. Both the anomalous τ curl and ENSO teleconnection mechanisms for KE variability are eliminated in the MD, leaving primarily the thermally driven component. This means that over the KE region, anywhere between 10% of SST variance in the west and 50% in the basin interior is forced by buoyancy fluxes. The remaining variability requires mechanical coupling either locally to induce anomalous Ekman advection and MLD processes or remotely, from mechanically coupled processes like ENSO or lagged SST responses to changes in gyre strength (Schneider et al. 2002).

Notice that the SST regression patterns differ (Figs. 5c,d), particularly the appearance of cold SSTA in a subtropical zonal band in the MD. In fact, the cool SSTAs in the NH subtropics are precisely where the MD variance increases in Fig. 2a. Section 4 explores why this region, as well as its SH counterpart, exhibit enhanced SSTA variability when momentum coupling is not permitted. Note that KE variability contributes to PDO SST variability (Schneider and Cornuelle 2005), which is discussed in more detail in section 5.

e. North Atlantic

The last region to highlight is the North Atlantic near 50°N where the northern flank of the subtropical gyre and southern flank of the subpolar gyre merge into a mean westerly flow. Associated with the subpolar gyre, the Labrador Current brings cold water southward while the Gulf Stream brings warm water northward as part of the subtropical gyre. SSTAs can form along the zonal gyre boundary resulting from variability in the τ driving Ekman advection, as well as depending on the strength of either gyre and changes in the latitudinal gyre boundary (Bjerknes 1964). Disconnecting the momentum coupling in this region reduces the SST variance by 35%–50%.

4. Increased SST variance

a. A mixed layer hypothesis

That the variance increases anywhere in Fig. 2a is a surprising result. A hypothesis for increased SST variance in the subtropics is that perhaps the MLD is shallower in the MD subtropics, resulting in increased SST variance via more efficient MLD temperature warming and cooling. This is a plausible hypothesis because the MLD is sensitive to τ forcing, yet the MD ocean experiences no anomalous τ-driven effects, resulting in reduced mixing from below and a potentially shallower MLD. The percent change in the annual mean MLD in Fig. 6 is calculated by $(\mathrm{MLD_{MD}} - \mathrm{MLD_{control}})/\mathrm{MLD_{control}}$ and confirms that the MLD is generally shallower when mechanically decoupled. Seasonal changes are evident, particularly in the North Pacific.

We demonstrate the effect of a shallower MLD via a simple one-dimensional Frankignoul and Hasselmann (1977)-type model of the form

$$\frac{dT}{dt} = -\frac{\lambda}{\rho c_o H} T + \frac{F}{\rho c_o H} = -aT + N, \qquad (2)$$

where T is mixed-layer temperature departure from climatology (equivalent to SST here), ρ is density, c_o is the specific heat of seawater, λT represents a linearization of

heat flux damping for a given temperature anomaly, F is atmospheric heat flux forcing, $a = -\lambda/\rho c_o H$ is the damping coefficient λ scaled by the heat capacity, and $N = F/\rho c_o H$ is the atmosphere heat flux forcing scaled by the heat capacity. It is easily shown (Frankignoul and Hasselmann 1977) that the resulting power spectrum for SST under the assumption of white atmospheric forcing with variance σ_N^2 is $P(\omega) = \sigma_N^2/(\omega^2 + a^2)$. Integrating over ω yields the resulting variance:

$$\sigma_T^2 = \frac{\pi\sigma_N^2}{2a} \sim \frac{1}{H}. \tag{3}$$

The percent change in variance then, varies negatively with the percent change in MLD [i.e. $d\ln(\sigma_T^2) = -d\ln(H)$], which shows that a decrease in MLD results in an increase in SST variance. This result is not necessarily intuitive, as a reduction in the thermal inertia ($\rho c_o H$) plays two roles: it increases the temperature variance through the "efficiency" of the heating [the second term on the right-hand side of (2)] but also reduces variance through increasing the effective damping rate [the first term in the right-hand side of (2)]. Equation (3) and its derivative show that the efficiency effect dominates.

Two problems arise when using this hypothesis to explain the increase in subtropical variance. First, the spatial structure of the percentage change in mean MLD (Fig. 6) is not consistent with the spatial structure of subtropical variance changes in Fig. 2a. For example, MLD shallowing is most pronounced poleward of regions with enhanced SST variance. Second, the percent change in MLD in the subtropics (about 5%–10% decrease) is much smaller than the percent change in SST variance (10%–30% increase). These inconsistencies imply that a different mechanism is responsible for the change in subtropical SST variance. Although the lack of anomalous τ driving on the ocean and the resulting change in the MD MLD cannot explain the SST variance results, the percentage change in MLD is consistent with the general warming pattern of the MD climatological SST compared to the control in Fig. 1. In general, the MD climatological SST is slightly warmer in regions where the MLD is shallower, presumably acting as a compensatory effect for the lack of anomalous τ driving.

On a separate note, the so-called reemergence mechanism (Alexander and Deser 1995; Alexander et al. 1999, 2001; Timlin et al. 2002; Deser et al. 2003) describes a MLD process by which temperature anomalies form in the deep MLD during NH winter, are sequestered under the shallower MLD during summer, and then resurface due to entrainment the following winter. Despite the shallower MLD, the annual cycle in the MD maintains a large seasonal variation that should support the reemergence mechanism.

b. An opposing flux hypothesis

For the off-equatorial regions of interest and away from dynamically active regions where vertical and deep ocean dynamics are important (e.g., ENSO, Atlantic meridional overturning circulation), SST variability is primarily driven by air–sea heat exchange and horizontal heat fluxes driven by Ekman advection (Alexander 1992). A second hypothesis for the change in SST variance in the midlatitudes and subtropics when momentum coupling is ignored is that in regions where anomalous thermal fluxes ($Q'_{\rm th}$) and Ekman fluxes ($Q'_{\rm ek}$) tend to negatively (positively) covary, the SST variance should increase (decrease) in the MD, as $Q'_{\rm ek} = 0$ by design. We will demonstrate through a simple analysis that in a given hemisphere, the zero-lag covariance of these two terms is dependent on the sign of the mean zonal wind.

Anomalous Ekman fluxes, assuming they are on the RHS of the temperature equation (i.e., a forcing term) are calculated by the following:

$$Q'_{\rm ek} \approx \left(\frac{1}{\rho f D_{\rm ek}}\right)\boldsymbol{\tau}' \times \nabla\overline{\rm SST}, \tag{4}$$

where $\boldsymbol{\tau}'$ consists of the zonal and meridional wind stress anomaly τ'_x and τ'_y, respectively, $D_{\rm ek}$ is the Ekman layer depth, ∇ is the horizontal gradient operator, and $\overline{\rm SST}$ is the annual cycle SST. Outside of the equatorial Pacific, $\nabla\overline{\rm SST}$ is generally equatorward, so for simplicity assume $\partial\overline{\rm SST}/dx \approx 0$. It follows that Ekman fluxes covary negatively with zonal wind variations as $Q'_{\rm ek} \propto \tau'_x/f \cdot \partial\overline{\rm SST}/dy$. Therefore, in the NH where $f > 0$ and $\nabla\overline{\rm SST} < 0$ or in the SH where $f < 0$ and $\nabla\overline{\rm SST} > 0$, we find that $Q'_{\rm ek} \propto -\tau'_x$.

In contrast, the bulk formulas for latent and sensible heat fluxes depend on the wind speed, and hence a linearization around the mean zonal wind yields

$$Q'_{\rm th} \approx \left.\frac{\partial Q_{\rm th}}{\partial u}\right|_{\overline{u}} u' = \frac{\overline{u}}{\overline{w}^2}\overline{Q_{\rm th}}u', \tag{5}$$

where $\overline{u}$ is the mean zonal wind, u' is the zonal wind anomaly, $\overline{w}$ is the mean wind speed, and $\overline{Q_{\rm th}}$ is mean latent heat flux which is always negative (out of the ocean). Unlike $Q'_{\rm ek}$, the variation of $Q'_{\rm th}$ with zonal wind anomalies, then, also depends on the sign of the mean zonal wind $\overline{u}$. As such, if $\overline{u}$ and u' are in phase, $Q'_{\rm th} < 0$ (heat going out of the ocean); however, if $\overline{u}$ and u' are out of phase, $Q'_{\rm th} > 0$ (heat going into the ocean). For instance, anomalous westerlies occurring in a mean westerly regime result in $Q'_{\rm th} < 0$ and $Q'_{\rm ek} < 0$, whereas

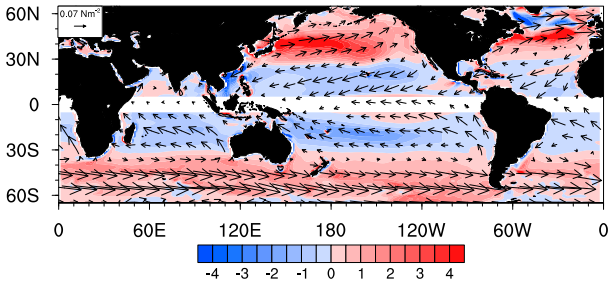

FIG. 7. Covariance between anomalous thermal fluxes Q'_{th} and Ekman fluxes Q'_{ek} (shaded) in CESM fully coupled control. Vectors show the CESM fully coupled control mean wind stress τ.

easterlies in a mean westerly regime result in $Q'_{th} > 0$ and $Q'_{ek} > 0$. Therefore, following Eqs. (4) and (5), Ekman fluxes tend to reinforce thermal fluxes in regions of mean westerly winds. Following the same logic, one can easily show that Ekman fluxes tend to oppose thermal fluxes in regions of mean easterly winds.

In the control, the covariance calculations and annual mean surface wind vectors in Fig. 7 reveal a negative covariance between Q'_{th} and Q'_{ek} in the subtropics where the mean winds are easterly and a positive covariance in the midlatitudes where the mean winds are westerly. A similar calculation for the MD is not necessary, as $Q'_{ek} = 0$ by design. Therefore, in the MD, the "damping" effect of Ekman fluxes on the $Q'_{th} + Q'_{th}$ variance in the subtropics is absent, which leads to a larger SST variance relative to the control as seen in Fig. 2a. The control Q'_{th} and Q'_{ek} variance maps are provided in Figs. 8a and 8b as to better visualize geographically where each term contributes as a forcing. Large Q'_{ek} variance occurs where $\partial\overline{SST}/dy$ is large (Fig. 1). As expected, regions of largest Q'_{ek} variance coincide with where SST variability is reduced in the MD (Fig. 2a). Regions of large Q'_{th} variance include the Kuroshio Current and Gulf Stream, both being large sources of heat loss to the atmosphere.

Overall, the inclusion of anomalous τ-driven effects dampens SSTA in the subtropics and enhances SSTA in the midlatitudes. Figure 9 provides a conceptual model to illustrate the connection between the mean zonal τ with an imposed anomaly and the net effect on the $Q'_{th} + Q'_{ek}$ variance in the MD CESM. In essence, the lack of Ekman flux damping of the thermal fluxes in the subtropics results in a larger $Q'_{th} + Q'_{ek}$ variance, which, we hypothesize, leads to larger SST variance. In contrast, in the midlatitudes where Ekman and thermal fluxes often reinforce one another, their collective variance is reduced, as well as the SST variance. Note that increased SST variance is less robust in the Atlantic subtropics. The Q'_{ek} variance is smaller to begin with in the Atlantic compared to the Pacific (Fig. 8a) such that

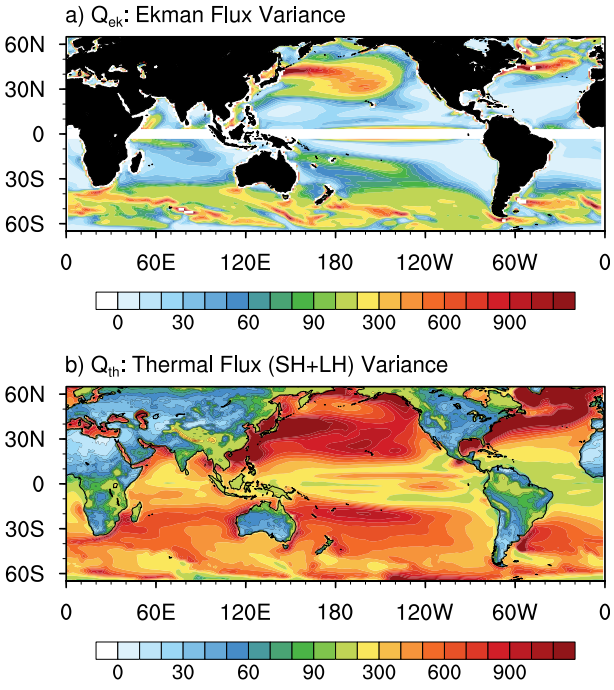

FIG. 8. (a) Ekman flux anomaly (Q'_{ek}) variance and (b) thermal flux anomaly (Q'_{th}) variance for CESM fully coupled control. Units are $(W\,m^{-2})^2$. Note that Q'_{ek} is masked out along the equator as f goes to zero.

Ekman fluxes contribute less to the $Q'_{th} + Q'_{ek}$ variance. Since Q'_{ek} plays a smaller role in the Atlantic forcing, allowing $Q'_{ek} = 0$ as in the MD has a lesser effect. A similar scenario occurs in the subtropical south Indian Ocean, where the Ekman flux variance is generally smaller than in the Pacific, leading to only small changes in the SST variance.

5. North Pacific SST variability

This section demonstrates how the MD SST variance response in the midlatitudes versus subtropics impacts the simulation of North Pacific SST variability. It is not new that Ekman fluxes contribute to North Pacific SST variability (Miller et al. 1994; Schneider et al. 2002; Alexander and Scott 2008), although studies often concentrate on the contribution from tropical forcing. In the fully coupled control, a portion of the Q'_{ek} contribution to the North Pacific SST variance is certainly due to ENSO teleconnections (Weare et al. 1976) and tropical forcing (Wallace and Gutzler 1981; Shukla and Wallace 1983) generating thermally driven SST anomalies via the "atmospheric bridge" (Alexander 1990, 1992; Lau and Nath 1994, 1996, 2001; Klein et al. 1999; Alexander et al. 2002) that are amplified via Ekman fluxes (Alexander and Scott 2008). SST variability in the MD, globally, is

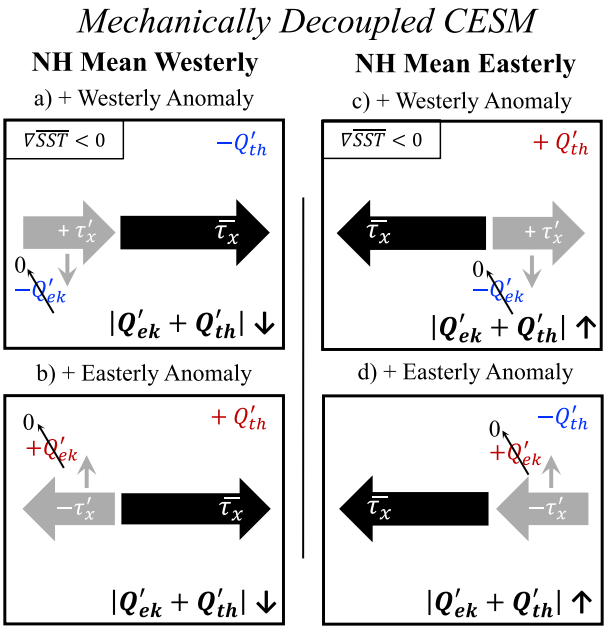

FIG. 9. Schematic outlining how the superposition of a zonal τ anomaly onto mean westerlies vs mean easterlies impacts the thermal and Ekman flux anomaly covariance in the NH in the MD. Assume $\overline{SST}$ increases equatorward or $\nabla\overline{SST} < 0$ in the NH. By design, $Q'_{ek} = 0$ in the MD. (a),(b) A zonal wind anomaly superimposed onto background westerlies generates Q'_{th} and Q'_{ek} that reinforce each other in the fully coupled control. With $Q'_{ek} = 0$ in the MD, $|Q'_{th} + Q'_{ek}|$ decreases, resulting in reduced SST variance in the midlatitudes when momentum coupling is ignored. (c),(d) A zonal wind anomaly superimposed onto background easterlies generates Q'_{th} and Q'_{ek} that oppose each other in the fully coupled control. When the Ekman fluxes are ignored in the MD, $|Q'_{th} + Q'_{ek}|$ increases because the Ekman fluxes do not cancel out any of the thermal fluxes, resulting in increased SST variance in the MD subtropics.

considered independent of tropical forcing as ENSO variability is absent. Next, we focus on how momentum coupling impacts PDO spatial structure.

The PDO is the dominant pattern of observed and modeled North Pacific SSTA (Mantua et al. 1997). Characterized by SSTA in the western-central North Pacific with opposite sign SSTA wrapping around the U.S. West Coast, the PDO pattern is considered an aggregate of variability that projects onto the same pattern (Schneider and Cornuelle 2005; Newman 2007; Newman et al. 2016). While the relative contribution of different sources of forcing that comprise PDO variability is not definitively settled, the sources themselves are widely studied, with contributions from the ENSO teleconnection to the North Pacific (Newman et al. 2003; Vimont 2005), atmosphere–ocean coupling (Latif and Barnett 1994) including variability in the KE (Deser et al. 1999; Seager et al. 2001; Wu et al. 2003; Kwon and Deser 2007), mixed-layer processes including "re-emergence" (Alexander and Deser 1995; Alexander et al. 2002), and atmospheric forcing (Frankignoul and Hasselmann 1977; Okumura 2013), particularly fluctuations in Aleutian low strength (Trenberth and Hurrell 1994; Mantua et al. 1997; Minobe 1997; Schneider et al. 2002). Using the interactive ensemble modeling strategy to isolate impacts of "noise" on the climate system, Yeh et al. (2007) demonstrate that atmospheric variability in both the tropics and locally in the North Pacific contribute to the SSTA variance. In the MD, Q'_{ek} cannot contribute to KE SST variability (see section 3d) and the ENSO teleconnection mechanism is absent. Therefore, North Pacific SST variability in the MD is primarily thermally driven via changes in atmospheric circulation.

Figure 10a shows the principal component time series (PC1) of the first empirical orthogonal function (EOF1) of unfiltered, area-weighted North Pacific SSTA computed over 20°–70°N, 100°E–100°W for the control. Note variability on multiple time scales, including decadal fluctuations and month-to-month changes indicative of the waxing and waning of the Aleutian low. The MD PC1 (Fig. 10b) does not look qualitatively different than the control. The percent variance explained by EOF1 is 23% in the control and 18% in the MD, although the total variances are not the same (Fig. 2a). The spatial patterns are generated by regressing SSTA onto the standardized PC1 time series. The control pattern (Fig. 10c) is analogous to the PDO SST pattern with warm SSTA in the east and cold SSTA extending from the west. As is typical, equatorial Pacific SST projects onto the PDO pattern (e.g., Di Lorenzo et al. 2015), resulting in a basinwide manifestation of the PDO referred to as the interdecadal Pacific oscillation (IPO; Power et al. 1999). The SSTA dipole pattern poleward of 30°N is similar in the MD (Fig. 10d), although with reduced amplitude because Q'_{ek} cannot reinforce the response. It is noteworthy that the PDO is the dominant variability even without ENSO forcing, confirming that the PDO is not solely a statistical artifact of the decadal modulation of ENSO or ENSO-forced reddening of the spectrum (Schneider and Cornuelle 2005).

Similarities end south of 30°N. No basinwide IPO pattern occurs in the MD, even when the SSTAs are low-pass filtered (not shown). Instead, the PDO pattern is robust, although meridionally confined in the extratropics. The lack of an IPO pattern is consistent with the Pacific climate variability null hypothesis proposed by Di Lorenzo et al. (2015), in that basinwide Pacific decadal variability is partly due to ENSO and partly due to stochastic atmospheric processes. The basinwide signal of the IPO is presumably due to ENSO variability (see also Newman et al. 2016), although it is unclear whether the pattern exists in the absence of ENSO. In

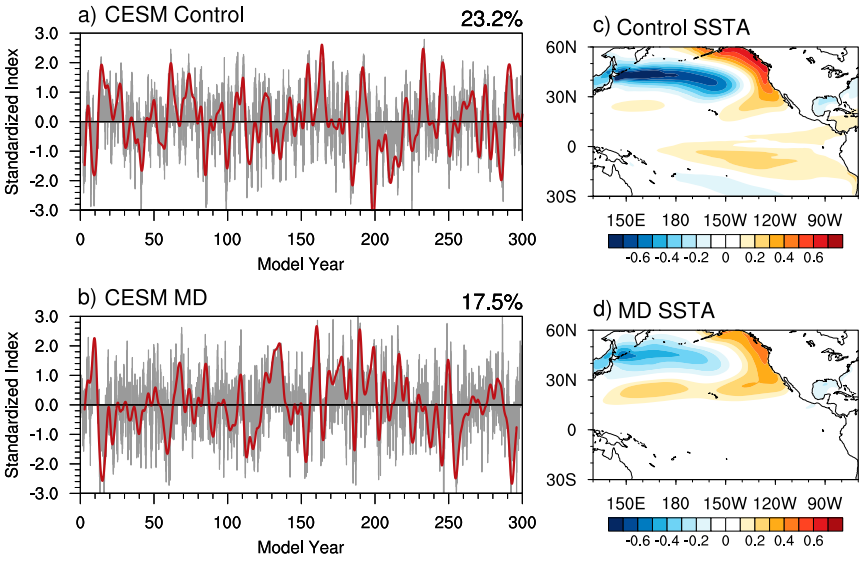

FIG. 10. (left) Standardized PC1 of the first EOF of North Pacific SSTA computed over domain 20°–70°N, 100°E–100°W, and (right) the SSTA regression pattern for (top) the CESM control and (bottom) the MD. Low-pass filtered (Lanczos filter with 13-yr cutoff) PC1 is shown in red. Units for the spatial pattern are °C per unit standard deviation of PC1. The variance explained by the first EOF is shown at the top right of each time series panel.

fact, Di Lorenzo et al. (2015) state that "more sophisticated coupled model experiments are needed to separate the fraction of decadal variability that is driven by ENSO versus MM [meridional modes]" (p. 9447). This is essentially what the MD does. The lack of an IPO in the MD suggests that without the ENSO piece, the tropical-to-extratropical interplay in their hypothesis rather unsurprisingly breaks down, thus implying that the ENSO piece is crucial for the basinwide pattern. As such, separating the ENSO component out in the MD presumably leaves the stochastically (thermally) forced component in the North Pacific, which projects onto the PDO pattern. That stochastic local atmospheric variability is crucial in simulating the full decadal North Pacific SSTA variance is also demonstrated through ensemble model experiments in Yeh and Kirtman (2004, 2006), as well as a role for nonlocal (e.g., tropical origin) in Yeh et al. (2007). No decadal filtering of the data is shown in this study, although as seen in Fig. 10b, the PDO signal is clearly lower frequency.

Also notable is the warm signal along the California west coast extending westward across the basin through the subtropics, similar to Fig. 5d. The lack of a subtropical band in the control PDO pattern suggests that Q'_{th} and Q'_{ek} associated with the PDO in the control nearly cancel each other out, leaving no substantial SSTA footprint. The MD PDO pattern reflects the SST variance ratio in Fig. 2a, with reduced amplitude variability stemming from the KE and enhanced variability in a zonal subtropical belt relative to the control. The pattern is also robust. The first EOF of SSTA computed over the full Pacific basin yields the same result.

6. Discussion

a. Summary

The relative effects of buoyancy versus momentum coupling on SST variance in climate models are not easily identifiable. SOMs, to some extent, separate the thermally coupled component but this approach often meets criticism because the role of ocean dynamics is ignored. In this study, a mechanically decoupled (MD) configuration of CESM is utilized to fill the gap in the model hierarchy between fully coupled and SOM versions and identify the extent to which momentum coupling influences SST variance. The MD is buoyancy (thermal + freshwater fluxes) coupled but also permits anomalous ocean mass transport decoupled from the anomalous τ. More simply, the MD does not include anomalous τ-driven effects on ocean circulation. SST variability arises via two mechanisms in the MD: 1) buoyancy fluxes and 2) anomalous ocean heat transport convergence decoupled from the anomalous τ. This is distinctly different from SOMs in which SST variability arises via thermal fluxes and the fully coupled in which SST variability arises via similar mechanisms as the MD plus the addition of anomalous

momentum fluxes. The SOM MLD is held constant, whereas the MD MLD varies seasonally and can respond to changes in ocean mass transport and seasonal τ. The fully coupled MLD also responds to anomalous τ.

Results show that momentum coupling is essential to simulating the fully coupled control SST variance in the tropics, subtropics, and midlatitudes (Fig. 2a). Without anomalous τ-driven effects, the equatorial Pacific SST variance decreases by 80%–90%, primarily due to the lack of ENSO. North Pacific variance, specifically the τ-sensitive Kuroshio–Oyashio Extension region, reduces from 50% in the interior basin to 90% off coastal Japan. The Southern Ocean between 40° and 60°S, where wind associated with the southern annual mode drives anomalous Ekman fluxes, experiences reduced SST variance. The boundary in the North Atlantic where the subtropical and subpolar gyres merge also shows reduced variance. Excluding anomalous momentum coupling has the opposite effect in the subtropics, with the MD simulating enhanced subtropical SST variance compared to the fully coupled control. Although the shallower mean MLD in the MD (Fig. 6) may play some role in the differences between the fully coupled and MD versions, we show through an analytical framework that the percent change in MLD is not consistent with the spatial structure or amplitude of subtropical SST variance changes.

Instead, we present an ''opposing flux hypothesis'' to explain the changes in SST variance when momentum coupling is ignored. Reduced (increased) SST variance in the MD occurs almost exclusively where the mean surface winds are westerly (easterly). A conceptual model (Fig. 9) summarizes the hypothesis. In a midlatitude westerly regime, anomalous zonal winds generate thermal (Q'_{th}) and Ekman (Q'_{ek}) fluxes that reinforce each other. In the MD, $Q'_{\text{ek}} = 0$, and therefore the variance of $Q'_{\text{th}} + Q'_{\text{ek}}$ decreases, resulting in reduced SST variance. In a subtropical easterly regime, thermal and Ekman fluxes oppose each other; therefore, since $Q'_{\text{ek}} = 0$ in the MD, Q'_{ek} does not cancel out any Q'_{th}, resulting in increased $Q'_{\text{th}} + Q'_{\text{ek}}$ variance and enhanced SST variance. The fully coupled control covariance of Q'_{th} and Q'_{ek} (Fig. 7) in the subtropics (midlatitudes) is negative (positive), supporting the hypothesis that opposing fluxes in the subtropics dampen the SST variability. As such, the lack of Ekman fluxes driving upper ocean temperature advection that opposes the thermally driven response leads to larger subtropical SST variability in a model without momentum coupling.

A by-product of disengaging the model's momentum coupling is the absence of ENSO variability (Larson and Kirtman 2015b), which allows us to investigate extratropical SST variability in the absence of momentum coupling *and* tropical forcing. Even without tropical forcing or momentum coupling, the PDO is the dominant North Pacific SST pattern in the MD. The thermally coupled PDO in the MD is meridionally confined poleward of 15°N with enhanced variability in a zonal subtropical band (Fig. 10d) that is not observed or simulated in the fully coupled control. The subtropical band is where Ekman fluxes typically oppose thermal fluxes in the control, therefore reducing the SST footprint. In the MD, SST variability in this region associated with the PDO increases because the thermal fluxes are unopposed by Ekman fluxes. No IPO structure is apparent in the MD, suggesting that the ENSO piece is essential for this basinwide pattern (Di Lorenzo et al. 2015).

b. *Implications for slab ocean model configurations*

Interpreting slab ocean model (SOM) results as what would be expected if a coupled model with both full atmosphere and ocean dynamics was only thermally coupled may be misleading. For example, in certain SOMs [for the CCSM4 version, see Bitz et al. (2012)], the prescribed MLD is from a fully coupled simulation and is not what one would expect from a thermally coupled version with mean ocean circulation (the MD). Instead, the MD MLD is shallower toward the poles compared to the control (Fig. 6), suggesting that the thermally coupled component of a fully coupled model is not perfectly represented in a slab ocean model. As such, interpreting SOM results should be done carefully as to not overstate its representativeness of the thermally coupled component of a fully coupled model.

Since mechanically decoupling CESM results in an increase of subtropical SST variance (Fig. 2a), it is possible that models without momentum coupling, including SOMs, may be overestimating subtropical SST variance. This is important for SOM studies highlighting Pacific meridional modes (e.g., Vimont et al. 2009; Zhang et al. 2014; Thomas and Vimont 2016), as they are characterized by subtropical SSTA. Neglecting Ekman fluxes in these studies may produce overly strong meridional mode SST variability compared to what would occur in a fully coupled model. Caution may be necessary in assessments of meridional mode variability and WES feedback strength in models that do not include momentum coupling. Additionally, clouds have been shown to be intimately linked to SSTA variability in the northeast subtropical Pacific via a positive low cloud–SST feedback, with ocean dynamics playing a damping role (Burgman et al. 2017). Determining the role of momentum coupling in this feedback is certainly of interest.

Of course, model-dependent results are always a concern when performing experiments with only one model. Of particular interest is whether models get this Ekman piece correct, as the MD shows that whether Ekman fluxes act as a damping or reinforcement is crucial to the SSTA variance. That said, our ability to build an intuitive conceptual model of why SST variance is enhanced (reduced) in the subtropics (midlatitudes) when CESM is mechanically decoupled suggests that this paradigm should hold true for other models that simulate realistic mean surface winds.

c. *Outlook for climate variability and change studies*

Determining the relative contributions of momentum versus buoyancy coupling to climate variability and change is a longstanding question (e.g., Zhang et al. 2015). For example, mean atmospheric surface circulation changes due to climate change could alter the covariance relationship between Ekman and thermal fluxes in a given location, particularly in the vicinity of the subtropics, and impact their combined influence on SST variance following the "opposing flux hypothesis" presented here. The role of τ-driven versus buoyancy-driven changes in ocean circulation and how they relate to sea level rise is also an especially relevant topic as the climate warms. Much of the uncertainty in model projected sea level rise (SLR) is attributed to the dynamic SLR response to variability in the Atlantic meridional overturning circulation (AMOC) or buoyancy fluxes (Yin et al. 2010; Church et al. 2013), although the role of anomalous τ-driven variability remains mostly unexplored. Preliminary analysis suggests that the low-frequency AMOC variability in CESM is almost entirely buoyancy driven, as the AMOC in the fully coupled CESM varies from the MD in only the τ-driven higher frequencies. Performing a MD framework with increasing CO_2 forcing could reveal clues as to what role, if any, τ variability plays in sea level rise projections.

Acknowledgments. This research was supported by the NOAA Climate and Global Change Postdoctoral Fellowship Program sponsored by the NOAA Climate Program Office and administered by the University Corporation for Atmospheric Research Cooperative Programs for the Advancement of Earth System Science (CPAESS). The authors also acknowledge computational support from the University of Miami Center for Computational Science. AC is supported by a NOAA Climate Program Office grant. BK is supported by NSF Grants AGS1558837, AGS1137911, OCE1499569, and OCE1559151.

REFERENCES

Alexander, M. A., 1990: Simulation of the response of the North Pacific Ocean to the anomalous atmospheric circulation associated with El Niño. *Climate Dyn.*, **5**, 53–65, https://doi.org/10.1007/BF00195853.

——, 1992: Midlatitude atmosphere–ocean interaction during El Niño. Part I: The North Pacific Ocean. *J. Climate*, **5**, 944–958, https://doi.org/10.1175/1520-0442(1992)005,0944:MAIDEN.2.0.CO;2.

——, and C. Deser, 1995: A mechanism for the recurrence of wintertime midlatitude SST anomalies. *J. Phys. Oceanogr.*, **25**, 122–137, https://doi.org/10.1175/1520-0485(1995)025,0122:AMFTRO.2.0.CO;2.

——, and J. D. Scott, 2008: The role of Ekman ocean heat transport in the Northern Hemisphere response to ENSO. *J. Climate*, **21**, 5688–5707, https://doi.org/10.1175/2008JCLI2382.1.

——, C. Deser, and M. S. Timlin, 1999: The reemergence of SST anomalies in the North Pacific Ocean. *J. Climate*, **12**, 2419–2433, https://doi.org/10.1175/1520-0442(1999)012,2419:TROSAI.2.0.CO;2.

——, M. S. Timlin, and J. D. Scott, 2001: Winter-to-winter recurrence of sea surface temperature, salinity and mixed layer depth anomalies. *Prog. Oceanogr.*, **49**, 41–61, https://doi.org/10.1016/S0079-6611(01)00015-5.

——, I. Bladé, M. Newman, J. R. Lanzante, N. C. Lau, and J. D. Scott, 2002: The atmospheric bridge: The influence of ENSO teleconnections on air–sea interaction over the global oceans. *J. Climate*, **15**, 2205–2231, https://doi.org/10.1175/1520-0442(2002)015<2205:TABTIO>2.0.CO;2.

——, D. J. Vimont, P. Chang, and J. D. Scott, 2010: The impact of extratropical atmospheric variability on ENSO: Testing the seasonal footprinting mechanism using coupled model experiments. *J. Climate*, **23**, 2885–2901, https://doi.org/10.1175/2010JCLI3205.1.

Anderson, B. T., 2007: On the joint role of subtropical atmospheric variability and equatorial subsurface heat content anomalies in initiating the onset of ENSO events. *J. Climate*, **20**, 1593–1599, https://doi.org/10.1175/JCLI4075.1.

Barsugli, J. J., and D. S. Battisti, 1998: The basic effects of atmosphere–ocean thermal coupling on midlatitude variability. *J. Atmos. Sci.*, **55**, 477–493, https://doi.org/10.1175/1520-0469(1998)055<0477:TBEOAO>2.0.CO;2.

Bates, S. C., B. Fox-Kemper, S. R. Jayne, W. G. Large, S. Stevenson, and S. G. Yeager, 2012: Mean biases, variability, and trends in air–sea fluxes and sea surface temperature in the CCSM4. *J. Climate*, **25**, 7781–7801, https://doi.org/10.1175/JCLI-D-11-00442.1.

Bitz, C. M., K. M. Shell, P. R. Gent, D. A. Bailey, G. Danabasoglu, K. C. Armour, M. M. Holland, and J. T. Kiehl, 2012: Climate sensitivity of the Community Climate System Model, version 4. *J. Climate*, **25**, 3053–3070, https://doi.org/10.1175/JCLI-D-11-00290.1.

Bjerknes, J., 1964: Atlantic air–sea interaction. *Advances in Geophysics*, Vol. 10, Academic Press, 1–82, https://doi.org/10.1016/S0065-2687(08)60005-9.

——, 1969: Atmospheric teleconnections from the equatorial Pacific. *Mon. Wea. Rev.*, **97**, 163–172, https://doi.org/10.1175/1520-0493(1969)097<0163:ATFTEP>2.3.CO;2.

Bladé, I., 1999: The influence of midlatitude ocean–atmosphere coupling on the low-frequency variability of a GCM. Part II: Interannual variability induced by tropical SST forcing. *J. Climate*, **12**, 21–45, https://doi.org/10.1175/1520-0442-12.1.21.

Blanke, B., J. D. Neelin, and D. Gutzler, 1997: Estimating the effect of stochastic wind stress forcing on ENSO irregularity.

J. Climate, **10**, 1473–1486, https://doi.org/10.1175/1520-0442(1997)010<1473:ETEOSW>2.0.CO;2.

Burgman, R. J., B. P. Kirtman, A. C. Clement, and H. Vazquez, 2017: Model evidence for low-level cloud feedback driving persistent changes in atmospheric circulation and regional hydroclimate. *Geophys. Res. Lett.*, **44**, 428–437, https://doi.org/10.1002/2016GL071978.

Capotondi, A., 2013: ENSO diversity in the NCAR CCSM4 climate model. *J. Geophys. Res. Oceans*, **118**, 4755–4770, https://doi.org/10.1002/jgrc.20335.

Chen, X., and J. M. Wallace, 2015: ENSO-like variability: 1900–2013. *J. Climate*, **28**, 9623–9641, https://doi.org/10.1175/JCLI-D-15-0322.1.

Chiang, J. C., and D. J. Vimont, 2004: Analogous Pacific and Atlantic meridional modes of tropical atmosphere–ocean variability. *J. Climate*, **17**, 4143–4158, https://doi.org/10.1175/JCLI4953.1.

Church, J. A., and Coauthors, 2013: Sea level change. *Climate Change 2013: The Physical Science Basis*, T. F. Stocker et al., Eds., Cambridge University Press, 1137–1216.

Clement, A., P. DiNezio, and C. Deser, 2011: Rethinking the ocean's role in the Southern Oscillation. *J. Climate*, **24**, 4056–4072, https://doi.org/10.1175/2011JCLI3973.1.

——, K. Bellomo, L. N. Murphy, M. A. Cane, T. Mauritsen, G. Rädel, and B. Stevens, 2015: The Atlantic multidecadal oscillation without a role for ocean circulation. *Science*, **350**, 320–324, https://doi.org/10.1126/science.aab3980.

Compo, G. P., and P. D. Sardeshmukh, 2010: Removing ENSO-related variations from the climate record. *J. Climate*, **23**, 1957–1978, https://doi.org/10.1175/2009JCLI2735.1.

Danabasoglu, G., S. C. Bates, B. P. Briegleb, S. R. Jayne, M. Jochum, W. G. Large, S. Peacock, and S. G. Yeager, 2012: The CCSM4 ocean component. *J. Climate*, **25**, 1361–1389, https://doi.org/10.1175/JCLI-D-11-00091.1.

Deser, C., M. A. Alexander, and M. S. Timlin, 1999: Evidence for a wind-driven intensification of the Kuroshio Current Extension from the 1970s to the 1980s. *J. Climate*, **12**, 1697–1706, https://doi.org/10.1175/1520-0442(1999)012<1697:EFAWDI>2.0.CO;2.

——, ——, and ——, 2003: Understanding the persistence of sea surface temperature anomalies in midlatitudes. *J. Climate*, **16**, 57–72, https://doi.org/10.1175/1520-0442(2003)016<0057:UTPOSS>2.0.CO;2.

——, and Coauthors, 2012: ENSO and Pacific decadal variability in the Community Climate System Model version 4. *J. Climate*, **25**, 2622–2651, https://doi.org/10.1175/JCLI-D-11-00301.1.

Di Lorenzo, E., G. Liguori, N. Schneider, J. C. Furtado, B. T. Anderson, and M. A. Alexander, 2015: ENSO and meridional modes: A null hypothesis for Pacific climate variability. *Geophys. Res. Lett.*, **42**, 9440–9448, https://doi.org/10.1002/2015GL066281.

DiNezio, P. N., and C. Deser, 2014: Nonlinear controls on the persistence of La Niña. *J. Climate*, **27**, 7335–7355, https://doi.org/10.1175/JCLI-D-14-00033.1.

——, L. J. Gramer, W. E. Johns, C. S. Meinen, and M. O. Baringer, 2009: Observed interannual variability of the Florida Current: Wind forcing and the North Atlantic Oscillation. *J. Phys. Oceanogr.*, **39**, 721–736, https://doi.org/10.1175/2008JPO4001.1.

Dommenget, D., 2010: The slab ocean El Niño. *Geophys. Res. Lett.*, **37**, L20701, https://doi.org/10.1029/2010GL044888.

Fan, M., and E. K. Schneider, 2012: Observed decadal North Atlantic tripole SST variability. Part I: Weather noise forcing and coupled response. *J. Atmos. Sci.*, **69**, 35–50, https://doi.org/10.1175/JAS-D-11-018.1.

Ferreira, D., C. Frankignoul, and J. Marshall, 2001: Coupled ocean–atmosphere dynamics in a simple midlatitude climate model. *J. Climate*, **14**, 3704–3723, https://doi.org/10.1175/1520-0442(2001)014<3704:COADIA>2.0.CO;2.

Frankignoul, C., 1985: Sea surface temperature anomalies, planetary waves, and air-sea feedback in the middle latitudes. *Rev. Geophys.*, **23**, 357–390, https://doi.org/10.1029/RG023i004p00357.

——, and K. Hasselmann, 1977: Stochastic climate models, Part II: Application to sea-surface temperature anomalies and thermocline variability. *Tellus*, **29**, 289–305, https://doi.org/10.3402/tellusa.v29i4.11362.

Gent, P. R., and Coauthors, 2011: The Community Climate System Model version 4. *J. Climate*, **24**, 4973–4991, https://doi.org/10.1175/2011JCLI4083.1.

Goodrich, G. B., 2007: Influence of the Pacific decadal oscillation on winter precipitation and drought during years of neutral ENSO in the western United States. *Wea. Forecasting*, **22**, 116–124, https://doi.org/10.1175/WAF983.1.

Gu, D.-F., and S. G. H. Philander, 1997: Interdecadal climate fluctuations that depend on exchanges between the tropics and extratropics. *Science*, **275**, 805–807, https://doi.org/10.1126/science.275.5301.805.

Hartmann, D. L., and F. Lo, 1998: Wave-driven zonal flow vacillation in the Southern Hemisphere. *J. Atmos. Sci.*, **55**, 1303–1315, https://doi.org/10.1175/1520-0469(1998)055<1303:WDZFVI>2.0.CO;2.

Hogg, A., M. P. Meredith, J. R. Blundell, and C. Wilson, 2008: Eddy heat flux in the Southern Ocean: Response to variable wind forcing. *J. Climate*, **21**, 608–620, https://doi.org/10.1175/2007JCLI1925.1.

Hurrell, J. W., and Coauthors, 2013: The Community Earth System Model: A framework for collaborative research. *Bull. Amer. Meteor. Soc.*, **94**, 1339–1360, https://doi.org/10.1175/BAMS-D-12-00121.1.

Jin, D., and B. P. Kirtman, 2009: Why the Southern Hemisphere ENSO responses lead ENSO. *J. Geophys. Res.*, **114**, D23101, https://doi.org/10.1029/2009JD012657.

Jin, F.-F., 1997: An equatorial ocean recharge paradigm for ENSO. Part I: Conceptual model. *J. Atmos. Sci.*, **54**, 811–829, https://doi.org/10.1175/1520-0469(1997)054<0811:AEORPF>2.0.CO;2.

Karnauskas, K. B., J. E. Smerdon, R. Seager, and J. F. González-Rouco, 2012: A Pacific centennial oscillation predicted by coupled GCMs. *J. Climate*, **25**, 5943–5961, https://doi.org/10.1175/JCLI-D-11-00421.1.

Kirtman, B. P., 1997: Oceanic Rossby wave dynamics and the ENSO period in a coupled model. *J. Climate*, **10**, 1690–1704, https://doi.org/10.1175/1520-0442(1997)010<1690:ORWDAT>2.0.CO;2.

——, and J. Shukla, 2002: Interactive coupled ensemble: A new coupling strategy for CGCMs. *Geophys. Res. Lett.*, **29**, 1367, https://doi.org/10.1029/2002GL014834.

——, and Coauthors, 2014: The North American multimodel ensemble: Phase-1 seasonal-to-interannual prediction; phase-2 toward developing intraseasonal prediction. *Bull. Amer. Meteor. Soc.*, **95**, 585–601, https://doi.org/10.1175/BAMS-D-12-00050.1.

Kleeman, R., J. P. McCreary, and B. A. Klinger, 1999: A mechanism for generating ENSO decadal variability. *Geophys. Res. Lett.*, **26**, 1743–1746, https://doi.org/10.1029/1999GL900352.

Klein, S. A., B. J. Soden, and N. C. Lau, 1999: Remote sea surface temperature variations during ENSO: Evidence for a tropical atmospheric bridge. *J. Climate*, **12**, 917–932, https://doi.org/10.1175/1520-0442(1999)012<0917:RSSTVD>2.0.CO;2.

Knutson, T. R. and S. Manabe, 1998: Model assessment of decadal variability and trends in the tropical Pacific Ocean. *J. Climate*,

11, 2273–2296, https://doi.org/10.1175/1520-0442(1998)011<2273:MAODVA>2.0.CO;2.

Kug, J. S., F. F. Jin, K. P. Sooraj, and I. S. Kang, 2008: State-dependent atmospheric noise associated with ENSO. *Geophys. Res. Lett.*, **35**, L05701, https://doi.org/10.1029/2007GL032017.

Kwon, Y. O., and C. Deser, 2007: North Pacific decadal variability in the Community Climate System Model version 2. *J. Climate*, **20**, 2416–2433, https://doi.org/10.1175/JCLI4103.1.

Larson, S. M., and B. Kirtman, 2013: The Pacific meridional mode as a trigger for ENSO in a high-resolution coupled model. *Geophys. Res. Lett.*, **40**, 3189–3194, https://doi.org/10.1002/grl.50571.

——, and B. P. Kirtman, 2014: The Pacific meridional mode as an ENSO precursor and predictor in the North American Multimodel Ensemble. *J. Climate*, **27**, 7018–7032, https://doi.org/10.1175/JCLI-D-14-00055.1.

——, and ——, 2015a: An alternate approach to ensemble ENSO forecast spread: Application to the 2014 forecast. *Geophys. Res. Lett.*, **42**, 9411–9415, https://doi.org/10.1002/2015GL066173.

——, and ——, 2015b: Revisiting ENSO coupled instability theory and SST error growth in a fully coupled model. *J. Climate*, **28**, 4724–4742, https://doi.org/10.1175/JCLI-D-14-00731.1.

——, and ——, 2017a: Drivers of coupled model ENSO error growth dynamics and the spring predictability barrier. *Climate Dyn.*, **48**, 3631–3644, https://doi.org/10.1007/s00382-016-3290-5.

——, and ——, 2017b: Linking preconditioning to extreme ENSO events and reduced ensemble spread. *Climate Dyn.*, 1–17, in press.

——, ——, and D. J. Vimont, 2017: A framework to decompose wind-driven biases in climate models applied to CCSM/CESM in the eastern Pacific. *J. Climate*, **30**, 8763–8782, https://doi.org/10.1175/JCLI-D-17-0099.1.

Latif, M., and T. P. Barnett, 1994: Causes of decadal climate variability over the North Pacific and North America. *Science*, **266**, 634–637, https://doi.org/10.1126/science.266.5185.634.

Lau, N.-C., and M. J. Nath, 1994: A modeling study of the relative roles of tropical and extratropical SST anomalies in the variability of the global atmosphere–ocean system. *J. Climate*, **7**, 1184–1207, https://doi.org/10.1175/1520-0442(1994)007<1184:AMSOTR>2.0.CO;2.

——, and ——, 1996: The role of the ''atmospheric bridge'' in linking tropical Pacific ENSO events to extratropical SST anomalies. *J. Climate*, **9**, 2036–2057, https://doi.org/10.1175/1520-0442(1996)009<2036:TROTBI>2.0.CO;2.

——, and ——, 2001: Impact of ENSO on SST variability in the North Pacific and North Atlantic: Seasonal dependence and role of extratropical sea–air coupling. *J. Climate*, **14**, 2846–2866, https://doi.org/10.1175/1520-0442(2001)014<2846:IOEOSV>2.0.CO;2.

——, and ——, 2003: Atmosphere–ocean variations in the Indo-Pacific sector during ENSO episodes. *J. Climate*, **16**, 3–20, https://doi.org/10.1175/1520-0442(2003)016<0003:AOVITI>2.0.CO;2.

Limpasuvan, V., and D. L. Hartmann, 1999: Eddies and the annular modes of climate variability. *Geophys. Res. Lett.*, **26**, 3133–3136, https://doi.org/10.1029/1999GL010478.

Liu, Z., 2012: Dynamics of interdecadal climate variability: A historical perspective. *J. Climate*, **25**, 1963–1995, https://doi.org/10.1175/2011JCLI3980.1.

Manabe, S., and R. J. Stouffer, 1996: Low-frequency variability of surface air temperature in a 1000-year integration of a coupled atmosphere–ocean–land surface model. *J. Climate*, **9**, 376–393, https://doi.org/10.1175/1520-0442(1996)009<0376:LFVOSA>2.0.CO;2.

Mantua, N. J., S. R. Hare, Y. Zhang, J. M. Wallace, and R. C. Francis, 1997: A Pacific interdecadal climate oscillation with impacts on salmon production. *Bull. Amer. Meteor. Soc.*, **78**, 1069–1079, https://doi.org/10.1175/1520-0477(1997)078<1069:APICOW>2.0.CO;2.

McCreary, J. P., Jr., and P. Lu, 1994: Interaction between the subtropical and equatorial ocean circulations: The subtropical cell. *J. Phys. Oceanogr.*, **24**, 466–497, https://doi.org/10.1175/1520-0485(1994)024<0466:IBTSAE>2.0.CO;2.

Meehl, G. A., A. Hu, J. M. Arblaster, J. Fasullo, and K. E. Trenberth, 2013: Externally forced and internally generated decadal climate variability associated with the interdecadal Pacific oscillation. *J. Climate*, **26**, 7298–7310, https://doi.org/10.1175/JCLI-D-12-00548.1.

Meredith, M., and A. Hogg, 2006: Circumpolar response of the Southern Ocean eddy activity to changes in the southern annular mode. *Geophys. Res. Lett.*, **33**, L16608, https://doi.org/10.1029/2006GL026499.

Miller, A. J., D. R. Cayan, T. P. Barnett, N. E. Graham, and J. M. Oberhuber, 1994: Interdecadal variability of the Pacific Ocean: Model response to observed heat flux and wind stress anomalies. *Climate Dyn.*, **9**, 287–302, https://doi.org/10.1007/BF00204744.

——, ——, and W. B. White, 1998: A westward-intensified decadal change in the North Pacific thermocline and gyre-scale circulation. *J. Climate*, **11**, 3112–3127, https://doi.org/10.1175/1520-0442(1998)011<3112:AWIDCI>2.0.CO;2.

Minobe, S., 1997: A 50–70 year climatic oscillation over the North Pacific and North America. *Geophys. Res. Lett.*, **24**, 683–686, https://doi.org/10.1029/97GL00504.

Neelin, J. D., M. Latif, and F. F. Jin, 1994: Dynamics of coupled ocean–atmosphere models: The tropical problem. *Annu. Rev. Fluid Mech.*, **26**, 617–659, https://doi.org/10.1146/annurev.fl.26.010194.003153.

Newman, M., 2007: Interannual to decadal predictability of tropical and North Pacific sea surface temperatures. *J. Climate*, **20**, 2333–2356, https://doi.org/10.1175/JCLI4165.1.

——, G. P. Compo, and M. A. Alexander, 2003: ENSO-forced variability of the Pacific decadal oscillation. *J. Climate*, **16**, 3853–3857, https://doi.org/10.1175/1520-0442(2003)016<3853:EVOTPD>2.0.CO;2.

——, and Coauthors, 2016: The Pacific decadal oscillation, revisited. *J. Climate*, **29**, 4399–4427, https://doi.org/10.1175/JCLI-D-15-0508.1.

Okumura, Y. M., 2013: Origins of tropical Pacific decadal variability: Role of stochastic atmospheric forcing from the South Pacific. *J. Climate*, **26**, 9791–9796, https://doi.org/10.1175/JCLI-D-13-00448.1.

Pierce, D. W., T. P. Barnett, N. Schneider, R. Saravanan, D. Dommenget, and M. Latif, 2001: The role of ocean dynamics in producing decadal climate variability in the North Pacific. *Climate Dyn.*, **18**, 51–70, https://doi.org/10.1007/s003820100158.

Power, S., T. Casey, C. Folland, A. Colman, and V. Mehta, 1999: Inter-decadal modulation of the impact of ENSO on Australia. *Climate Dyn.*, **15**, 319–324, https://doi.org/10.1007/s003820050284.

Qiu, B., 2003: Kuroshio Extension variability and forcing of the Pacific decadal oscillations: Responses and potential feedback. *J. Phys. Oceanogr.*, **33**, 2465–2482, https://doi.org/10.1175/2459.1.

Rodgers, K. B., P. Friederichs, and M. Latif, 2004: Tropical Pacific decadal variability and its relation to decadal modulations of ENSO. *J. Climate*, **17**, 3761–3774, https://doi.org/10.1175/1520-0442(2004)017<3761:TPDVAI>2.0.CO;2.

Rogers, J. C., and H. van Loon, 1982: Spatial variability of sea level pressure and 500 mb height anomalies over the Southern Hemisphere. *Mon. Wea. Rev.*, **110**, 1375–1392, https://doi.org/10.1175/1520-0493(1982)110<1375:SVOSLP>2.0.CO;2.

Schneider, N., and B. D. Cornuelle, 2005: The forcing of the Pacific decadal oscillation. *J. Climate*, **18**, 4355–4373, https://doi.org/10.1175/JCLI3527.1.

——, A. J. Miller, and D. W. Pierce, 2002: Anatomy of North Pacific decadal variability. *J. Climate*, **15**, 586–605, https://doi.org/10.1175/1520-0442(2002)015<0586:AONPDV>2.0.CO;2.

Schopf, P. S., and R. J. Burgman, 2006: A simple mechanism for ENSO residuals and asymmetry. *J. Climate*, **19**, 3167–3179, https://doi.org/10.1175/JCLI3765.1.

Screen, J. A., N. P. Gillett, D. P. Stevens, G. J. Marshall, and H. K. Roscoe, 2009: The role of eddies in the Southern Ocean temperature response to the southern annular mode. *J. Climate*, **22**, 806–818, https://doi.org/10.1175/2008JCLI2416.1.

Seager, R., Y. Kushnir, N. H. Naik, M. A. Cane, and J. Miller, 2001: Wind-driven shifts in the latitude of the Kuroshio–Oyashio Extension and generation of SST anomalies on decadal timescales. *J. Climate*, **14**, 4249–4265, https://doi.org/10.1175/1520-0442(2001)014<4249:WDSITL>2.0.CO;2.

Shukla, J., and J. W. Wallace, 1983: Numerical simulation of the atmospheric response to equatorial Pacific sea surface temperature anomalies. *J. Atmos. Sci.*, **40**, 1613–1630, https://doi.org/10.1175/1520-0469(1983)040<1613:NSOTAR>2.0.CO;2.

Solomon, A., J. P. McCreary Jr., R. Kleeman, and B. A. Klinger, 2003: Interannual and decadal variability in an intermediate coupled model of the Pacific region. *J. Climate*, **16**, 383–405, https://doi.org/10.1175/1520-0442(2003)016<0383:IADVIA>2.0.CO;2.

Stevenson, S., B. Fox-Kemper, M. Jochum, R. Neale, C. Deser, and G. Meehl, 2012: Will there be a significant change to El Niño in the twenty-first century? *J. Climate*, **25**, 2129–2145, https://doi.org/10.1175/JCLI-D-11-00252.1.

Thomas, E. E., and D. J. Vimont, 2016: Modeling the mechanisms of linear and nonlinear ENSO responses to the Pacific meridional mode. *J. Climate*, **29**, 8745–8761, https://doi.org/10.1175/JCLI-D-16-0090.1.

Thompson, D., and J. Wallace, 2000: Annular mode in the extratropical circulation. Part I: Month-to-month variability. *J. Climate*, **13**, 1000–1016, https://doi.org/10.1175/1520-0442(2000)013<1000:AMITEC>2.0.CO;2.

Timlin, M. S., M. A. Alexander, and C. Deser, 2002: On the reemergence of North Atlantic SST anomalies. *J. Climate*, **15**, 2707–2712, https://doi.org/10.1175/1520-0442(2002)015<2707:OTRONA>2.0.CO;2.

Trenberth, K. E., and J. W. Hurrell, 1994: Decadal atmosphere–ocean variations in the Pacific. *Climate Dyn.*, **9**, 303–319, https://doi.org/10.1007/BF00204745.

——, G. W. Branstator, D. Karoly, A. Kumar, N. C. Lau, and C. Ropelewski, 1998: Progress during TOGA in understanding and modeling global teleconnections associated with tropical sea surface temperatures. *J. Geophys. Res.*, **103**, 14 291–14 324, https://doi.org/10.1029/97JC01444.

Vimont, D. J., 2005: The contribution of the interannual ENSO cycle to the spatial pattern of decadal ENSO-like variability. *J. Climate*, **18**, 2080–2092, https://doi.org/10.1175/JCLI3365.1.

——, D. S. Battisti, and A. C. Hirst, 2001: Footprinting: A seasonal connection between the tropics and mid-latitudes. *Geophys. Res. Lett.*, **28**, 3923–3926, https://doi.org/10.1029/2001GL013435.

——, ——, and ——, 2003: The seasonal footprinting mechanism in the CSIRO general circulation models. *J. Climate*, **16**, 2653–2667, https://doi.org/10.1175/1520-0442(2003)016<2653:TSFMIT>2.0.CO;2.

——, M. Alexander, and A. Fontaine, 2009: Midlatitude excitation of tropical variability in the Pacific: The role of thermodynamic coupling and seasonality. *J. Climate*, **22**, 518–534, https://doi.org/10.1175/2008JCLI2220.1.

Wallace, J. M., and D. S. Gutzler, 1981: Teleconnections in the geopotential height field during the Northern Hemisphere winter. *Mon. Wea. Rev.*, **109**, 784–812, https://doi.org/10.1175/1520-0493(1981)109<0784:TITGHF>2.0.CO;2.

Weare, B. C., A. R. Navato, and R. E. Newell, 1976: Empirical orthogonal analysis of Pacific sea surface temperatures. *J. Phys. Oceanogr.*, **6**, 671–678, https://doi.org/10.1175/1520-0485(1976)006<0671:EOAOPS>2.0.CO;2.

Weijer, W., and Coauthors, 2012: The Southern Ocean and its climate in CCSM4. *J. Climate*, **25**, 2652–2675, https://doi.org/10.1175/JCLI-D-11-00302.1.

Wu, L., Z. Liu, R. Gallimore, R. Jacob, D. Lee, and Y. Zhong, 2003: Pacific decadal variability: The tropical Pacific mode and the North Pacific mode. *J. Climate*, **16**, 1101–1120, https://doi.org/10.1175/1520-0442(2003)16<1101:PDVTTP>2.0.CO;2.

Wu, R., and B. P. Kirtman, 2005: Roles of Indian and Pacific Ocean air–sea coupling in tropical atmospheric variability. *Climate Dyn.*, **25**, 155–170, https://doi.org/10.1007/s00382-005-0003-x.

Xie, S.-P., and S. G. H. Philander, 1994: A coupled ocean–atmosphere model of relevance to the ITCZ in the eastern Pacific. *Tellus*, **46A**, 340–350, https://doi.org/10.3402/tellusa.v46i4.15484.

Yeh, S. W., and B. P. Kirtman, 2004: Tropical Pacific decadal variability and ENSO amplitude modulation in a CGCM. *J. Geophys. Res.*, **109**, C11009, https://doi.org/10.1029/2004JC002442.

——, and ——, 2006: Origin of decadal El Niño–Southern Oscillation–like variability in a coupled general circulation model. *J. Geophys. Res.*, **111**, C01009, https://doi.org/10.1029/2005JC002985.

——, ——, and S.-I. An, 2007: Local versus non-local atmospheric weather noise and the North Pacific SST variability. *Geophys. Res. Lett.*, **34**, L14706, https://doi.org/10.1029/2007GL030206.

Yin, J., S. M. Griffies, and R. J. Stouffer, 2010: Spatial variability of sea level rise in twenty-first-century projections. *J. Climate*, **23**, 4585–4607, https://doi.org/10.1175/2010JCLI3533.1.

Zebiak, S. E., and M. A. Cane, 1987: A model El Niño–Southern Oscillation. *Mon. Wea. Rev.*, **115**, 2262–2278, https://doi.org/10.1175/1520-0493(1987)115<2262:AMENO>2.0.CO;2.

Zhang, H., A. Clement, P. Di Nezio, 2014: The South Pacific meridional mode: A mechanism for ENSO-like variability. *J. Climate*, **27**, 769–783, https://doi.org/10.1175/JCLI-D-13-00082.1.

Zhang, R.-H., L. M. Rothstein, and A. J. Busalacchi, 1998: Origin of upper-ocean warming and El Niño change on decadal scale in the tropical Pacific Ocean. *Nature*, **391**, 879–883, https://doi.org/10.1038/36081.

——, C. Gao, X. Kang, H. Zhi, Z. Wang, and L. Feng, 2015: ENSO modulations due to interannual variability of freshwater forcing and ocean biology-induced heating in the tropical Pacific. *Sci. Rep.*, **5**, 18506, https://doi.org/10.1038/srep18506.

——, R. Sutton, G. Danabasoglu, T. L. Delworth, W. M. Kim, J. Robson, and S. G. Yeager, 2016: Comment on "The Atlantic Multidecadal Oscillation without a role for ocean circulation." *Science*, **352**, 1527, https://doi.org/10.1126/science.aaf1660.

Zhang, Y., J. M. Wallace, and D. S. Battisti, 1997: ENSO-like interdecadal variability: 1900–93. *J. Climate*, **10**, 1004–1020, https://doi.org/10.1175/1520-0442(1997)010<1004:ELIV>2.0.CO;2.